Advances in Military Technology
Vol. 20, No. 1, 2025, pp. 277-295
ISSN 1802-2308, eISSN 2533-4123
DOI 10.3849/aimt.01967

Design and Validation of a Low Frequency Anti-Vibration Mount using NBR-Carbon Fiber Composite

K. Shajahan[1*], R. S. A. Sundar[1], A. V. R. Kumar[1] and J. Reji[2]

[1] *DRDO-Naval Physical & Oceanographic Laboratory, Thrikkakara, Kochi, Kerala, India*
[2] *Cochin University of Science and Technology, Kochi, Kerala, India*

The manuscript was received on 5 February 2025 and was accepted after revision for publication as an original research paper on 6 June 2025.

Abstract:

The vibrations generated by onboard machinery can adversely impact stealth of marine platforms. Designers typically mitigate the source of vibration; however additional passive anti-vibration mounts have to be used for isolating equipment above a specific frequency threshold. This study focuses on the development, testing, and comparative evaluation of composite anti-vibration mounts incorporating short carbon fiber reinforcement in an NBR matrix. Three damping elements designs were optimized based on the stress-strain properties of five NBR compositions with varying short-fiber loading. The research involved designing and testing the mounts, FEM of the materials, FEA of the mounts, and experimental validation. Among the tested designs, model-2 with 2 parts per hundred rubber (phr) fiber loading demonstrated superior vibration damping performance for low-frequency applications.

Keywords:

vibration isolation, composite anti-vibration mount, transmissibility, nitrile rubber, low-frequency mount, finite element modeling, creep

1 Introduction

The vibrations generated by onboard machinery in ships and submarines can have detrimental effects on crew well-being, reduce equipment lifespan, and critically interfere with the vessel's communication systems, thereby compromising its stealth capabilities. Mitigating vibrations at the source is the primary objective of system designers. However, due to the complexity of integrating multiple systems on board, the use of additional vibration isolation solutions is often necessary.

In such scenarios, passive anti-vibration mounts serve as an effective method to mitigate the adverse effects of vibrations produced by various machinery [1-6]. A high

* *Corresponding author: DRDO-Naval Physical & Oceanographic Laboratory, Thrikkakara, Kochi, Kerala, IN-682 021, India. Phone: +91 94 46 20 13 81, +91 48 42 42 48 58, E-mail: shajahan-k.npol@gov.in. ORCID 0009-0000-9022-0274.*

static stiffness and low dynamic stiffness with S shaped legs for improved vibration damping and isolation was discussed by Hung Vu et al. [7]. The development of these mounts involves diverse design and material considerations, depending on factors such as load rating, type of loading, required isolation frequency, and the working environment [8]. Chai et al. discussed various quasi-zero stiffness systems with high-static and low-dynamic stiffness to attenuate low-frequency vibration [9]. The synergistic effect of graphene nanoplates and carbon black within styrene-butadiene rubber to enhance both mechanical properties and vibration damping characteristics was reported by Chandramohan et al. [10]. Utilization of glass and carbon fiber in engine mounts was discussed by Jaiswal et.al [11]. Literature on composite anti-vibration mount based on short carbon fiber in nitrile rubber is scarce. A composite anti-vibration mount, developed in this study using short carbon fiber reinforced nitrile rubber, was designed to support a load rating of 220 kg and effectively isolate vibrations at frequencies above 25 Hz. Our literature review revealed that no such studies were made previously.

The design process begins with modeling the mount using computational tools, incorporating constraints such as load capacity, dimensional limitations, permissible static deflection, and desired isolation frequency. The use of Mooney-Rivlin model constants to analyze anti-vibration mounts and predict deflections under various compressive loads was studied by Suryatal et al. [12]. The selection of materials and fiber loading, based on damping requirements, hardness, and the environmental conditions in which the mount will operate, has been discussed elsewhere [13-15]. In this study, a rubber matrix was used as the primary material, reinforced with short carbon fibers at varying loading percentages.

Material testing was conducted to determine the mechanical and damping properties, which were subsequently used for material modeling in finite element analysis (FEA) [12, 16]. The uniaxial tensile mechanical behavior of randomly distributed short-cut CF/NBR composites reported by Zhao et al. [17] is of relevance to present study. The static deflection and harmonic behavior of the designed mount were analyzed using FEA. Following the analytical phase, the mounts were fabricated and subjected to mechanical and dynamic testing to evaluate their vibration transmissibility, isolation characteristics, and energy dissipation (hysteresis loss). These evaluations facilitated a comparative study of the performance of the developed mounts.

2 Design of Vibration Isolation Mounts

Mount design is based on several critical factors, including geometric constraints, load rating, required static deflection, resonance and isolation frequencies, damping requirements, and environmental conditions [8, 18]. The geometric constraints for the mount include footprint requirements, height, and overall size limitations, determined by the equipment mounted on top of the mount. The load rating for the mount was set at 220 kg.

The objective was to develop a mount with the dimensions of $(150 \times 120 \times 60)$ mm, achieving a resonance frequency of less than 20 Hz at the specified load while providing effective vibration isolation above 25 Hz. The allowable deformation under a 220 kg load was specified as (1.0 ± 0.2) mm.

The mount design was developed using SOLIDWORKS$^{\mathrm{TM}}$ software and comprised several components: the float, elastomeric stack, casing, bottom plate, and encapsulation. The details were discussed in an Indian patent that was filed [19]. The float, casing, and bottom plate were constructed from stainless steel (SS), while the elastomeric stack was made of a rubber composite with varying fiber loading. The encapsulation was created using a commercial polyurethane (PU) sealant.

To reduce dynamic stiffness, three different designs for the damping stacks incorporating perforations were developed (as shown in Fig. 1). The materials properties of compositions 1-5 (Tab. 1) were used to evaluate these designs. The design that exhibited the lowest resonance frequency and deformation within the range of (1.0 ± 0.2) mm was selected for final analysis. Figs 1a and 1b illustrate the schematic views of the selected design and its components prepared for final validation. The characterization of the materials used for the design was previously detailed by Shajahan et al. [10, 20].

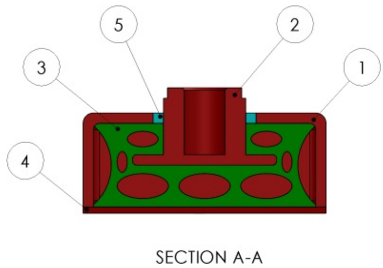

(a)

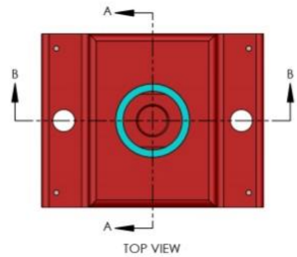

(b)

Fig. 1 Schematic of Design (a) Section View, showing 1: Damping Stack, 2: Float, 3: Casing, 4: Bottom Plate and 5: PU Sealant (b) Top view

3 Materials and Methodology

The float, casing, and bottom plate were fabricated using SS316 stainless steel, as illustrated in Fig. 1. The elastomeric stack was composed of a nitrile rubber (NBR) composite with neat and carbon fiber loading, as detailed in Tab. 1. These composites were prepared using a two-roll mill, as previously studied by Shajahan et al. [20]. The edge sealing of the mount was achieved using a commercially available ether-based polyurethane (PU) sealant.

Rubber samples with specific compositions were molded into sheets and button samples. These samples were cured at 160 °C for an optimal duration, determined through rheometric studies, and subsequently used for various testing purposes. The same compositions were also utilized for molding the final damping elements in the composite anti-vibration mount.

Tab. 1 Mount samples

NBR Compound	Comp. 1	Comp. 2	Comp. 3	Comp. 4	Comp. 5
Carbon Short Fibre ~3 mm [phr]	–	0.5	1.0	2.0	4.0

3.1 Material Testing

Material characterization was performed to evaluate properties such as density, hardness, modulus of elasticity, ultimate tensile strength (UTS), tear strength, and compression set, following ASTM standards [21-24]. Tensile properties were evaluated using dumbbell shaped Type-C specimens with a speed of 500 mm/min as per ASTM D412. The mean values of 5 specimens were reported. The density of the materials was measured using a densimeter, while hardness was determined using a Bareiss fully automatic rubber hardness tester Digitest II, Shore A module. Tensile and tear specimens were punched from 2 mm thick sheets using a die, prepared according to ASTM standards, and tested on a universal testing machine. The data obtained from these tests were used to determine mechanical properties such as ultimate tensile strength, percentage elongation, modulus of elasticity at various elongations, and tear strength, as shown in Tab. 2. The details were discussed in [20].

Tab. 2 Physical and mechanical stress-strain properties [20]

Property, standard, Unit	**Comp. 1**	**Comp. 2**	**Comp. 3**	**Comp. 4**	**Comp. 5**
Hardness, ASTM D2240, Shore A	72.38	73.5	73.81	75.68	80.15
Density, ASTM D4052, g/cm^3	1.226	1.273	1.257	1.274	1.272
Tensile strength, ASTM D412, MPa	12.80	12.54	13.03	13.53	12.25
M100, ASTM D412, MPa	3.26	3.46	3.75	4.03	4.68
M200, ASTM D412, MPa	6.47	6.77	7.28	7.42	8.33
M300, ASTM D412, MPa	9.74	10.06	10.48	10.64	10.76
EB, ASTM D412, %	444	432	418	411	391

The glass transition temperatures (Tg) of the compositions, measured using differential scanning calorimeter (DSC) and dynamic mechanical analysis (DMA), are presented in Tab. 3. These values correspond to standard literature values. Additionally, the tan delta values of all compositions are also listed in Tab. 3. Fig. 2 illustrates the tan delta versus frequency plot for all compositions obtained through DMA-TTS (Dynamic Mechanical Analysis – Time Temperature Superposition). The maximum tan δ value of 1.2736 was observed for the 2 phr loading, which was subsequently chosen for the final molding of the mount. It seems the critical fiber loading for increased tand δ ceases above 2 phr fiber loading. The critical fiber loading due to stick-slip phenomena in short fiber composites was reported by Treviso et. al. [25]. The values of tan δ increase with fiber incorporation was reported by Geethamma et. al. [26]. The glass transition temperature obtained from DSC remained largely unchanged with increasing fiber loading, which aligns with findings from earlier studies [27-29].

Tab. 3 Thermal analysis results

Property	**Standard**	**Comp. 1**	**Comp. 2**	**Comp. 3**	**Comp. 4**	**Comp. 5**
DSC Tg, °C	ASTM D3418	−27.27	−27.95	−27.42	−27.04	−27.57
DMA Tg, °C	ASTM D4065	−30.01	−27.90	−11.47	−11.57	−10.58
DMA Tanδ	ASTM D4065	1.13	0.7519	0.8326	1.2736	1.0783

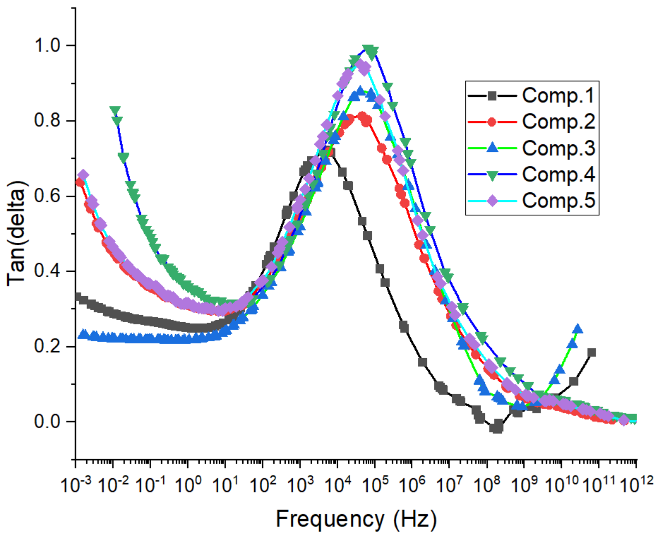

Fig. 2 Tan δ vs frequency of compounds 1-5

3.2 Material Analysis and Modeling Using FEA

Material properties need to be defined properly in the simulation software to accurately analyze a prototype made from non-linear materials. Non-linear materials, such as polymer composites, are not typically pre-defined in material libraries. In this study, polymer composites with hyperelastic and viscoelastic behavior were analyzed. The hyperelastic properties were defined using strain energy density functions, while the viscoelastic properties were characterized using the Prony series.

For hyperelastic material modeling, experimental uni-axial tensile test data was utilized for hyperelastic curve fitting in ANSYS Workbench. The uni-axial test data was imported into the hyperelastic modeling module, where various hyperelastic models were fitted to the experimental data. The model with the least fitting error was selected, and the curve-fitting process was used to derive the hyperelastic material constants.

The hyperelastic curve-fitted data for the different samples, along with the corresponding strain energy density functions, were used as input for static structural and harmonic analysis of the mounts. The Mooney-Rivlin two-parameter model was identified as the most suitable for defining the hyperelastic properties of the elastomeric samples [30]. The Mooney-Rivlin parameter constants for samples 1-5 are presented in Tab. 4.

3.3 Mount Analysis Using FEA

Material modeling was conducted as a prerequisite for analyzing the mount prototype using finite element analysis (FEA) tools. The final mount geometry was created and imported into the FEA software, where the material properties were assigned to the various components of the mount. The analysis included static structural analysis, Eigen frequency (or modal) analysis, transmissibility analysis using frequency domain studies, and hysteresis analysis using the transient module [31]. Appropriate boundary conditions, such as fixed constraints, force constraints, and directional constraints, were applied. The meshing process ensured a uniform, high-quality mesh with low skewness.

Harmonic analysis of the mounts was performed using the frequency domain module in COMSOL Multiphysics [32]. The mount geometry was imported into the software, material properties were assigned to the respective components, and boundary conditions were applied. The bottom base plate was fixed, and a predefined acceleration of 1 g (9.81 m/s²) was applied in the vertical upward direction. To measure the acceleration transmissibility of the mounts, two accelerometer probes were attached – one at the top of the weight and the other at the bottom base plate. A frequency sweep ranging from 1 to 500 Hz was applied to the system, and the resulting frequency vs. transmissibility curve was obtained.

3.4 Molding of Mount

The mounts were fabricated using molds designed to meet the geometric specifications of $(150 \times 120 \times 60)$ mm. The matrix material for molding the damping stack consisted of rubber compounds with varying fiber loading, as detailed in Tab. 1. The damping elements were manufactured using a transfer molding technique.

The molded damping element, encapsulated with the rubber composition, was subsequently inserted into a metallic casing. All internal interfaces within the casing were bonded to the damping stack using a commercial polyurethane (PU) sealant, which was cured at room temperature for 24 hours. The completed mounts were then tested for various characteristics.

3.5 Testing of Mounts

The final molded prototypes were tested to evaluate their mechanical and dynamic behavior. Key parameters such as deflection, hysteresis, and creep at the rated load of 220 kg were analyzed using a universal testing machine (UTM). The static deflection of the mount at the rated load was determined by compressing the prototypes under a 220 kg load at a loading rate of 5 mm/min during the compression test [33]. Hysteresis loss was measured by subjecting the mounts to cyclic loading and unloading between zero and the rated load for ten cycles. The corresponding hysteresis graph was plotted, and the damping capability of the mount was determined from the hysteresis loss value during the 10^{th} cycle. Tab. 6 summarizes the properties obtained for both the damping stack and mounts (Models 1-5) made with Composition 4.

The permanent set value of the mounts was determined by compressing the mounts to the rated load between two flat plates using a UTM. After maintaining the load for 72 hours, the load was removed, and the mounts were allowed to relax for 24 hours. The difference between the initial and final heights provided the permanent set value.

Vibration properties, including natural frequency, peak transmissibility, and isolation frequency, were measured using an electrodynamic shaker [33]. The mounts were installed on the shaker using a base plate, and weights were applied to the top of the mounts as shown in Fig. 3. Random and harmonic vibration signals were applied to the shaker table over a frequency range of 10 - 1 000 Hz. The corresponding properties were measured, and results for vibration properties under loads of 152 kg (in the *x*, *y*, and *z* axes) and 190 kg (in the *z*-axis) are presented in Tab. 7. The table also includes attenuation values for velocity between the top and bottom of the mounts at 1 000 Hz for comparison.

Long-term creep behavior was analyzed by applying the rated load to the top of the mounts and recording the deflection over time until the change became negligible. Ageing studies were conducted using diesel and hot water baths. For diesel ageing, the mounts were immersed in diesel for 72 hours, after which the weight change was measured to determine the diesel absorption percentage [33]. The mounts were also immersed in hot water baths at various temperatures, and changes in water absorption, deflection, hysteresis values, and vibration properties were studied.

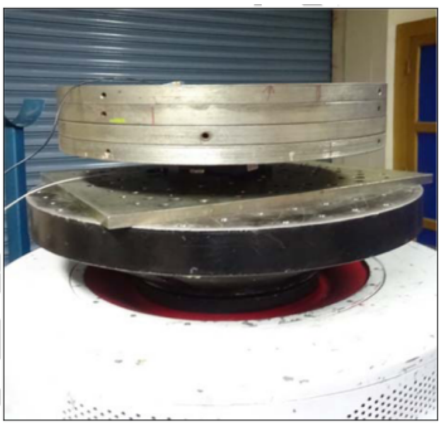

Fig. 3 Vibration test of mount on exciter head with 152 kg *dead load in z axis* [9]

4 Results and Discussion

Fig. 4a presents the uni-axial stress-strain curves for Samples 1-5, and Fig. 4b depicts the typical curve-fitting process performed for Sample 2. The Mooney-Rivlin parameter constants determined for each compound are summarized in Tab. 4. The model gives good agreement with experimental results as reported by other authors [30, 34].

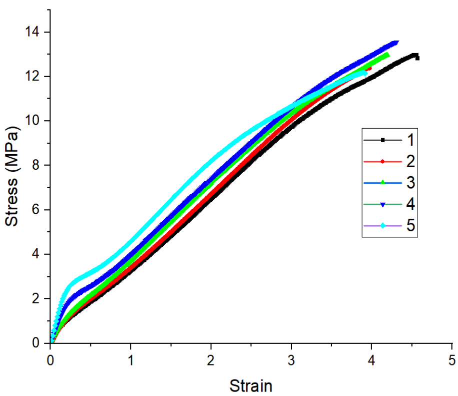

(a)

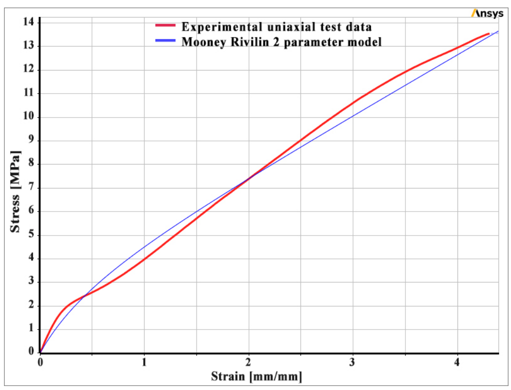

(b)

Fig. 4 (a) Stress strain curves of compounds1-5, (b) Curve fitting of tensile data using Mooney-Rivlin 2 parameter model for compound 4

Tab. 4 Mooney-Rivlin two parameter constants for different material samples.

Sl. No.	Material Property [MPa]
Compound 1	$C_{10} = 1.553741$
	$C_{01} = -0.0988279$
Compound 2	$C_{10} = 0.95103$
	$C_{01} = 2.46691$
Compound 3	$C_{10} = 1.0652049$
	$C_{01} = 1.578555$
Compound 4	$C_{10} = -0.2949227$
	$C_{01} = 5.461627$
Compound 5	$C_{10} = 32.9476$
	$C_{01} = -17.2791$

Figs 5-7 present the static analysis results, including von Mises stress distribution and deformation, for damping stack models 1, 2, and 3, respectively, utilizing Composition 4. Tab. 5 summarizes the static deflection values under a 220 kg load and the resonance frequencies for a 152 kg load. The results indicate that Model 2 with Composition 4 achieves the lowest resonance frequency while maintaining an acceptable static deflection of (1 ± 0.4) mm. Similar studies were reported by Keliang et al. [35]. Based on these findings, Model 2 with Composition 4 was selected for further validation studies.

Figs 8a and 8b compare the simulation results with experimental data for static deflection under a 220 kg load and harmonic analysis at a 152 kg load, respectively. The results demonstrate that the FEM-predicted values for static deflection closely align with the experimental data for the selected mount 4 with deviation of 6.48 % more than the FEM values. For other mounts the deviations between experimental and FEM values in deflection varies from 3.57 % to 25.25 %. Fig. 8b depicts the resonance values obtained for mounts 1-5, with the damping stack composed of Composition 4. The resonance values also show a strong correlation with the experimental data with a variation of 0 %-7.41 %, also reported by Suryatal et al. [12].

Fig. 9 illustrates the harmonic analysis results, depicting transmissibility as a function of frequency for mounts 1 to 5. The data indicate that mount 4 exhibits the lowest resonance frequency, a result that was further validated through experimental testing.

Tab. 5 Simulation results for static deformation and resonance

Model	Static Deformation at 220 kg	Natural Frequency at 152 kg
Model-1	0.475 mm	23 Hz
Model-2	0.851 mm	19 Hz
Model-3	0.692 mm	21 Hz

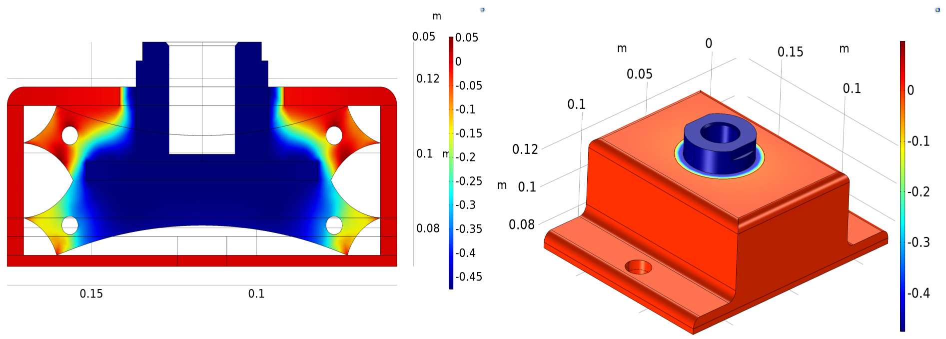

(a) *(b)*

Fig. 5 (a) Model-1: Von Mises stress distribution, (b) Static deflection

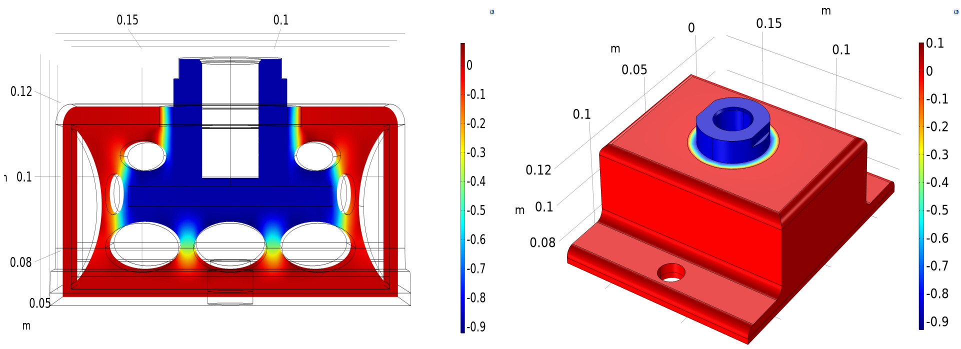

(a) *(b)*

Fig. 6 (a) Model-2: Von Mises stress distribution, (b) Static deflection

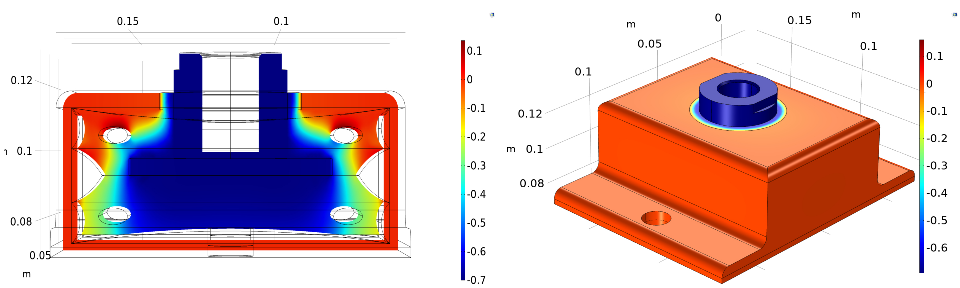

(a) *(b)*

Fig. 7 (a) Model-3: Von Mises stress distribution, (b) Static deflection

DOI 10.3849/aimt.01967

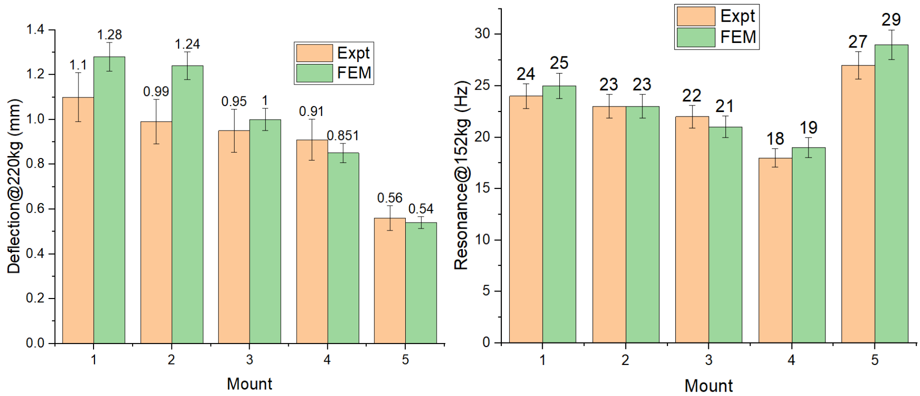

(a) *(b)*

Fig. 8 (a) Comparison of FEM and Experimental values static deflection,
(b) Comparison of FEM and Experimental values resonance

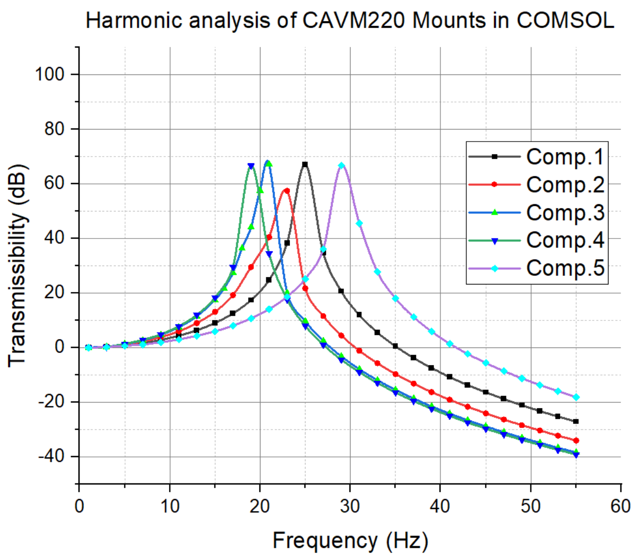

Fig. 9 Comparison of Resonance frequencies in FEM

The molded damping stacks had initially been tested for static deflection at a 220 kg load using a UTM, and the results were presented in Tab. 6 and illustrated in Fig. 10a. The data reveal a linear decrease in deflection as the fiber loading increases in agreement with reported literatures [10-11]. Once the damping stacks were integrated into the casing and finished, the mount deflection was reduced to approximately one-third of the bare stack values which is also normal due to restricted boundary conditions reported by Wang et. al [36].

The creep values of the mounts decreased up to mount 4, which contained 2 phr of fiber loading, after which an increase was observed for mount 5, as shown in Fig. 10b. Notably, mount 4 exhibited creep within the acceptable range, remaining below 30 %.

The hysteresis properties of the damping stacks and mounts are summarized in Tab. 6 and illustrated in Fig. 11a. Among the tested mounts, mount 4 exhibited the highest hysteresis, indicating superior damping characteristics. Similar study was reported by Qian et al. [37].

Additionally, the permanent set values, evaluated according to [13], were found to be the lowest for mount 4, which was fabricated with a 2 phr fiber loading was shown in Fig. 11b.

Tab. 7 presents the dynamic properties of the molded mounts which are illustrated in Figs 12-14. The vibration-damping properties of the mounts were evaluated along the *x*, *y*, and *z* axes under an applied load of 152 kg for comparison. Additionally, unfilled and 2 phr fiber-filled mounts were tested under a 190 kg load in the *z*-axis, which is the primary axis of application. The results confirmed that the mount with 2 phr fiber loading exhibited the lowest resonance frequency and provided superior low-frequency isolation as shown in Fig. 12a.

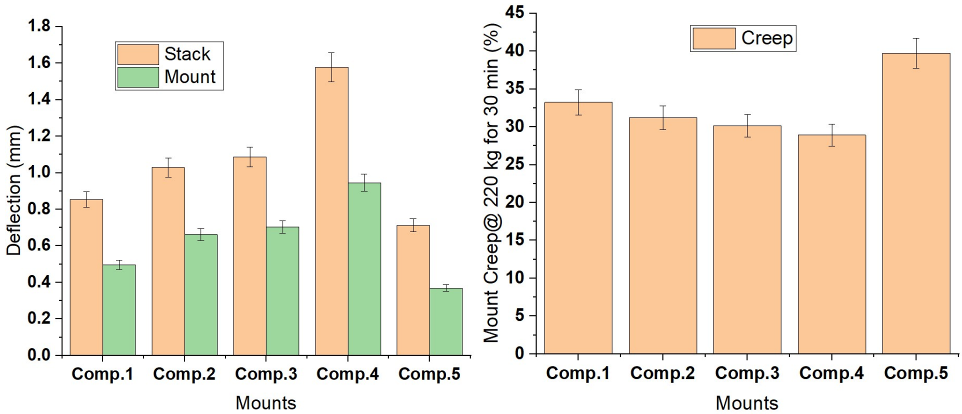

(a) (b)

Fig. 10 (a) Stack and mount deflection at 220 kg*, (b) Mount creep at* 220 kg *for* 30 min

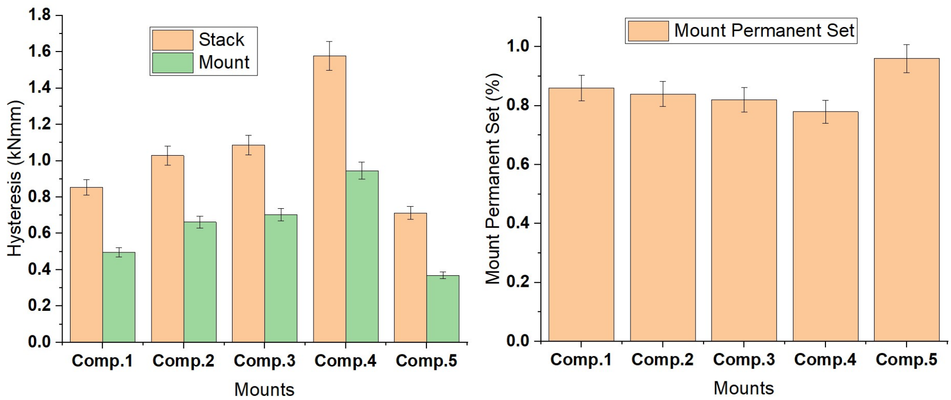

(a) (b)

Fig. 11 (a) Stack and mount hysteresis 0-220 kg*,*
(b) Permanent set of mount at 220 kg *for* 72 h [33]

Tab. 6 Properties of Damping stack and molded mounts

Property	**Unit**	**Standard**	**Comp. 1**	**Comp. 2**	**Comp. 3**	**Comp. 4**	**Comp. 5**
Stack Deflection at 220 kg	mm	Custom	3.74	3.38	3.36	2.86	2.22
Mount Deflection at 220 kg	mm	Custom	1.1	0.99	0.95	0.91	0.56
Mount Creep at 220 kg for 30 min	%	Custom	33.23	31.21	30.14	28.9	39.7
Stack Hysteresis	kNmm	Custom	0.8541	1.0283	1.0870	1.5774	0.7133
Mount Hysteresis	kNmm	Custom	0.4969	0.6623	0.7028	0.9451	0.3688
Mount Hysteresis	%		24.72	25.79	26.06	30.32	22.71
Mount Permanent Set 72 h at 220 kg	%	Custom	0.86	0.84	0.82	0.78	0.96

Tab. 7 Vibration properties of molded mounts

Mount Reso-nance	Hz	**Axis, weight**	**Comp.1**	**Comp.2**	**Comp.3**	**Comp.4**	**Comp.5**
		z, 152 kg	24	23	22	18	27
		z, 190 kg	17.7	—	—	15	—
		x, 152 kg	21	24	26	25	29
		y, 152 kg	33	29	36	31	38
Transmissibility Peak	dB	*z*, 152 kg	14.3	13	13	12.7	13
		z, 190 kg	12.7	—	—	12.0	—
		x, 152 kg	7.5	8	8.6	7.2	8
		y, 152 kg	7.8	8.7	8.1	3.1	7
Isolation	Hz	*z*, 152 kg	35	33	31	25	39
		z, 190 kg	25	—	—	21	—
		x, 152 kg	29	33	37	35	41
		y, 152 kg	46	41	51	40	53
Max Isolation	dB	*z*, 152 kg	–55	–58	–56	–60	–55
		z, 190 kg	–67	—	—	–67	—
		x, 152 kg	–59.1	–58.7	–57.4	–56.5	–54.1
		y, 152 kg	–46	–57	–55	–60	–54
%Attenuation at 1 000 Hz	%	*z*, 152 kg	83.04	88.7	91.52	92.12	81.56

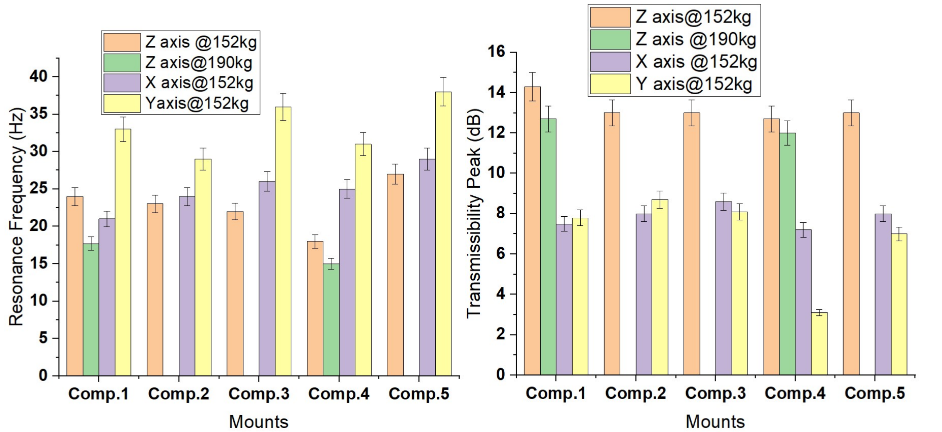

(a) (b)

Fig. 12 (a) Resonance frequency of mounts in z, x and y axes at 152 kg *and* 190 kg *loads, (b) Peak transmissibility of mounts at* 152 kg *and* 190 kg *loads* [33]

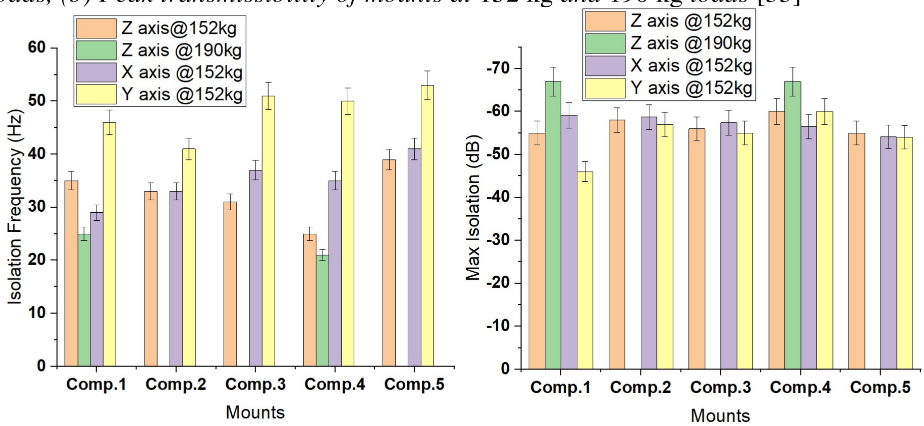

(a) (b)

Fig. 13 (a) Isolation frequency of mounts in z, x and y axes at 152 kg *and* 190 kg *loads, (b) Maximum Isolation of mounts at* 152 kg *and* 190 kg *loads*

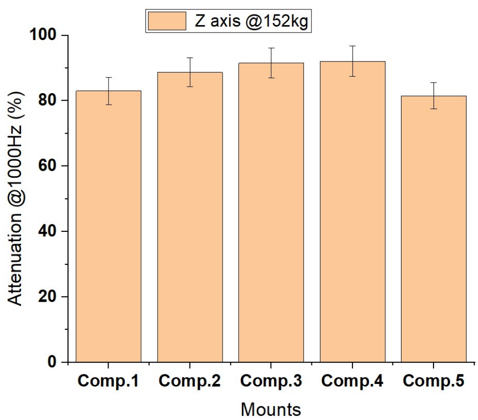

Fig. 14 Attenuation of mounts in z axes at 152 kg *load*

Fig. 15a illustrates the load-deflection curves of mount 4 under a 220 kg load, showing a linear response within the acceptable limits for the intended application [10-11]. Fig. 15b depicts the hysteresis loop of mount 4, highlighting a hysteresis loop area of 30 % for the mount with 2 phr fiber loading. Fig. 16a compares the hysteresis loops of mounts 1-5, fabricated with different compositions, while Fig. 16b presents a histogram of the hysteresis loop areas for these mounts. These results demonstrate the superior damping and isolation characteristics of mount 4 with 2 phr fiber loading. Similar results reported elsewhere also. [36-37].

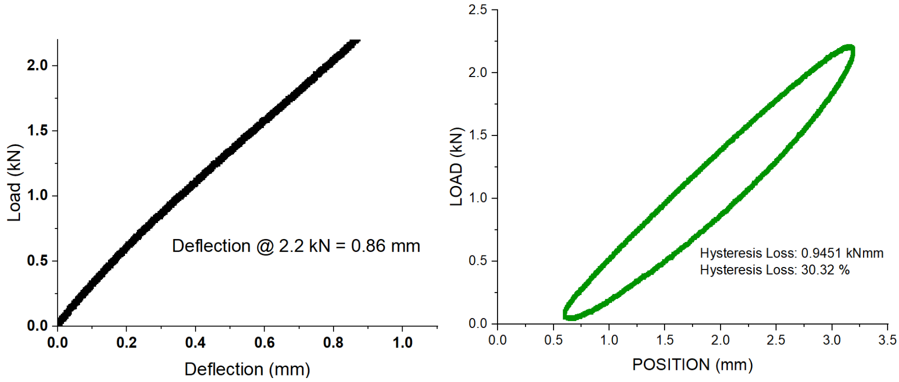

(a) *(b)*

Fig. 15 (a) Load vs Deflection of mount 4, (b) Hysteresis plot of mount 4

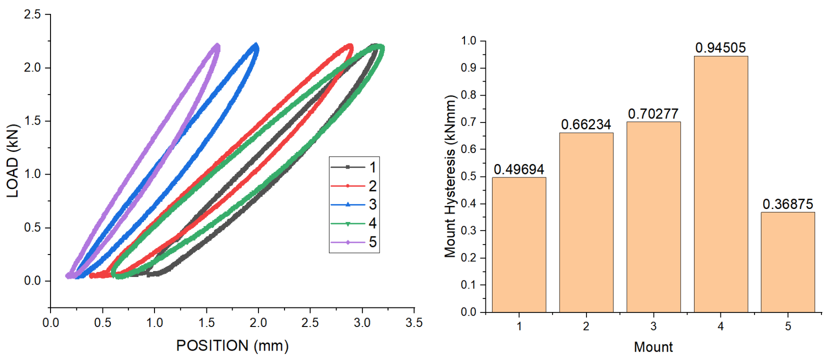

(a) *(b)*

Fig. 16 (a) Hysteresis loops of mounts molded with compounds 1 to 5 [19],
(b) Comparison of hysteresis loop area

Fig. 17 illustrates the vibration transmissibility behavior of mounts 1 to 5 under a 152 kg load on the Z-axis. It is evident that mount 4, with 2 phr fiber loading, exhibits the lowest resonance frequency and the highest damping performance. Fig. 18 compares the vibration transmissibility curves of mounts 1 and 4 under a 190 kg dead load in the *z*-axis, further highlighting the advantageous effect of the 2 phr fiber-loaded configuration in mount 4. Fig. 19 presents the comparison of vibration attenuation at 1 000 Hz, in terms of velocity as specified in references [21, 33], for mounts fabricated with Compound 4 under 190 kg and 152 kg dead loads in the *x*, *y*, and *z* axes. These results strongly support the effectiveness of mount 4 for low-frequency vibration isolation applications. Tab. 8 showed the comparative properties of existing anti-vibration mounts and mount 4. The benefits of the proposed solution, in terms of cost-effectiveness, performance, and ease of maintenance were clearly evident.

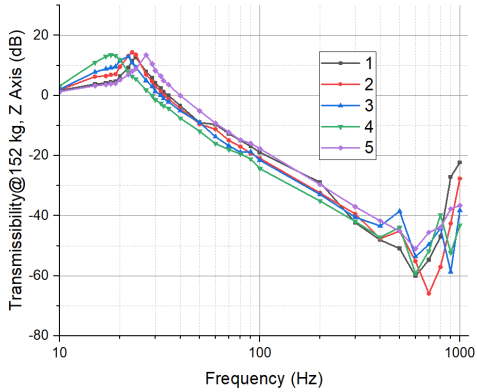

Fig. 17 Vibration Transmissibility plot of mounts 1-5 at 152 kg *dead load in z axis*

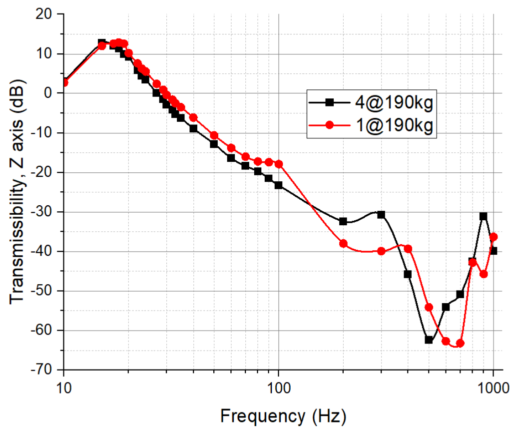

Fig. 18 Comparison of Vibration transmissibility of mount molded with compound 1 & 4 *in z axis with* 190 kg *dead load* [9]

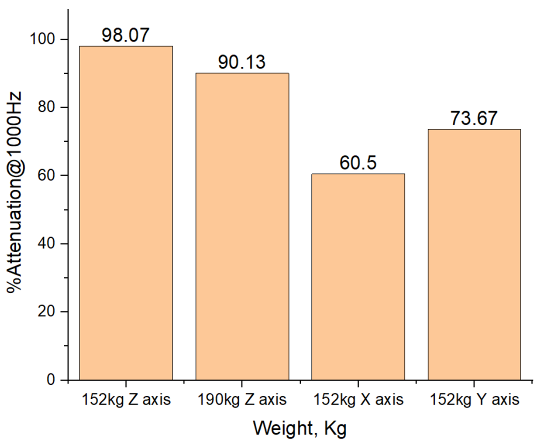

Fig. 19 Comparison of Vibration attenuation in terms of velocity of mount molded with compound 4 *in z axis with* 190 *and* 152 kg *dead load in x, y and z axis*

Tab. 8 Comparative Values of Comp-4 mount with commercial equivalent mounts

Sl. No.	Parameter	Mount 4	Existing
1	Dimensions, L × W × H, [mm]	150 × 118 × 60	150 × 118 × 60
2	Capacity of single mount, [kg]	220	220
3	Material	Stainless Steel 316 / NBR-CF composite	Mild Steel / Rubber
4	Weight, [g]	2 400 ± 100	2 500 ± 300
5	Deflection at 220 kg, [mm]	1.5 ± 0.3	1.0 ± 0.4
7	Vibration Transmissibility as per QAP, [dB]	< 14 (peak max)	< 14 (peak max)
8	Resonance peak, single mount, [Hz]	15 ± 1	33 ± 3
9	Isolation frequency, [Hz]	from 30 onwards	from 55 onwards
10	Fatigue at 5 Hz	> 1 00 000 cycles	na
11	Shelf Life, [years]	> 5	< 3
12	Estimated Service Life	> 9	~5
13	Oil/Diesel/Water Resistance	Outstanding	Limited
14	Replacement	Composite part only	Entire mount
15	Cost	INR20 000/-	INR30 000/-

5 Conclusion

- The objective of this project was to develop a mount capable of achieving low-frequency isolation under a 220 kg load, with specific dimensional constraints of (150 × 120 × 60) mm. The results demonstrated that the finite element model values closely aligned with experimental data for both deflection and harmonic analysis. Model 2 exhibited the lowest natural frequency of 19 Hz under a 152 kg load, which was corroborated by the experimental value of 18 Hz. Consequently, this model was selected for investigating the effect of varying fiber loading.
- Among the mounts tested, mount 4, containing 2 % fiber loading, demonstrated the lowest resonance and isolation frequencies, making it the best-performing mount. Further increases in fiber loading beyond 2 % were found to be unfavorable, as they resulted in increased resonance and isolation frequencies. Additionally, the peak transmissibility at resonance remained relatively unaffected by variations in fiber loading.
- In conclusion, mount 4, with 2 % fiber loading, is determined to be the optimal choice among the five mounts for low-frequency isolation applications for equipment with resonances above 25 Hz which cannot be achieved by existing mounts having similar footprints.

- Scope of future study includes extensive environmental testing to evaluate the long-term durability of the mounts in harsh marine conditions such as exposure to salt water, extreme temperatures, long-term vibration endurance and fatigue strength.

Acknowledgments

The authors wish to acknowledge the Director, NPOL for granting permission to publish this work.

References

[1] LU, X., X. LI, and M. TIAN. Preparation of High Damping Elastomer with Broad Temperature and Frequency Ranges Based on Ternary Rubber Blends. *Polymers for Advanced Technologies,* 2014, **25**(1), pp. 21-28. DOI 10.1002/pat.3199.

[2] CORSARO, R.D, and H. SPERLING, eds. *Sound and Vibration Damping with Polymers*. Washington: American Chemical Society, 1990. ISBN 0-8412-1778-5.

[3] WU, C.F., Y. OTANI, N. NAMIKI, H. EMI, K.H. NITTA and S. KUBOTA. Dynamic Properties of an Organic Hybrid of Chlorinated Polyethylene and Hindered Phenol Compound. *Journal of Applied Polymer Science*, 2001, **82**(7), pp. 1788-1793. DOI 10.1002/app.2021.

[4] VARGHESE, H., T. JOHNSON, S.S. BHAGWAN, S. JOSEPH, S. THOMAS and G. GROENINCKX. Dynamic Mechanical Behavior of Acrylonitrile Butadiene Rubber/Poly(ethylene-*co*-vinyl acetate) Blend. *Journal of Polymer Science, Part B*, 2002, **40**(15), pp. 1556-1570. DOI 10.1002/polb.10204.

[5] PETROSIAN, L.G. Vibration Damage and Vibration Control Measures. In: *Dynamics of Structures.* Cham: Springer, 2024, pp. 535-548. DOI 10.1007/978-3-031-63539-7_20.

[6] KOROBIICHUK, I., V. MEL'NICK, V. KOSOVA, V. PAVLENKO and K. BURSACOV. Study of Systems of Active Vibration Protection of Navigation Instrument Equipment. *Applied System Innovation*, 2024, **7**(5), 95. DOI 10.3390/asi7050095.

[7] VU, M.H., N.P.V. BACH, T.N. LUONG and T.B. TRUNG. Kinematics Design and Statics Analysis of Novel 6-DOF Passive Vibration Isolator with S-Shaped Legs Based on Stewart Platform. *Journal of Vibroengineering*, 2023, **26**(1), pp. 66-78. DOI 10.21595/jve.2023.23511.

[8] REN M., X. XIE and Z. ZHANG. Investigation on a New Passive Active Vibration Isolator. In: *26th International Congress on Sound and Vibration*. Montreal: ICSV, 2019, pp 7-11.

[9] CHAI Y., J. BIAN and M. LI. A Novel Quasi-Zero-Stiffness Isolation Platform via Tunable Positive and Negative Stiffness Compensation Mechanism. *Nonlinear Dynamics*, 2024, **112**(1), pp. 101-123. DOI 10.1007/s11071-023-09018-0.

[10] CHANDRAMOHAN, S., M. VAITHIYANATHAN, B.C. CHAKRABORTY and M.M. DHARMARAJ. Synergistic Effect of Graphene and Carbon Black on the Mechanical and Vibration Damping Characteristics of Styrene-Butadiene Rubber. *Iranian Polymer Journal,* 2025, **34**, pp. 17-27. DOI 10.1007/s13726-024-01349-y.

[11] JAISWAL P. and S. BARVE. Utilization of Composite Materials for Engine Mounts & Different Vehicle Structures: A Review. *AIP Conference Proceedings*, 2022, **2421**(1), 040007. DOI 10.1063/5.0078199.

[12] SURYATAL B.K., P.K. AMBADEKAR, J.S. GAWANDE, K.A. MAHAJAN, V.K. JAVANJAL, M.M. SONEKAR, R.N. YERRAWAR and S.H. GAWANDE. Deflection Prediction of an Anti-Vibration Mount by Finite Element Analysis. *Mathematical Modelling of Engineering Problems,* 2024, **11**(6), pp. 1452-1456. DOI 10.18280/mmep.110606.

[13] CHAKRABORTY, B.C. and D. RATNA. *Polymers for Vibration Damping Applications*. New York: Elsevier, 2020. ISBN 0-12-819252-6.

[14] AKANDE, I.G., M.A. FAJOBI, O.A. ODUNLAMI and O.O. OLUWOLE. Exploitation of Composite Materials as Vibration Isolator and Damper in Machine Tools and Other Mechanical Systems: A Review. *Materials Today: Proceedings*, 2021, **43**(2), pp. 1465-1470. DOI 10.1016/j.matpr.2020.09.300.

[15] ABHILASH, S.S. and D.L. SINGARAVELU. Effect of Fiber Content on Mechanical, Morphological and Vibration Damping Characteristics of Natural Fiber-reinforced Composite Fuel Tanks. *Journal of Natural Fibers*, 2022, **19**(16), pp. 14994-15007. DOI 10.1080/15440478.2022.2069629.

[16] PIERSOL, A.G. and T.L. PAEZ. *Harris' Shock and Vibration Handbook*. 6th ed. New York: McGraw-Hill Companies, 2010. ISBN 978-0071508193 6.

[17] ZHAO, W.L., Y. LIU, Z.C. DONG and X.J. YU. Establishment of Strain Rate-dependent Intrinsic Models for Short-Cut Carbon Fiber/Nitrile Composites in Different Pyrolysis States. *Polymer Composite,* 2024, **45**(9), pp. 8321-8334. DOI 10.1002/pc.28343.

[18] CHUNG, D.D.L. Review Materials for Vibration Damping. *Journal of Materials Science*, 2001, **36**, pp. 5733-5737. DOI 10.1023/A:1012999616049.

[19] SHAJAHAN, K., R.S. ARUN SUNDAR, T. BEJOY and A.V. RAMESH KUMAR. *Composite Anti-Vibration Mount with Improved Elastomeric Composite Stack for Enhanced Low-Frequency Damping. Indian Patent (Filed).* Application No. 202411075627, 2024.

[20] SHAJAHAN, K., R.S. ARUN SUNDAR, A.V. RAMESH KUMAR and J. REJI. Investigations on Short Carbon Fibre Filled NBR Composites for Fabrication of Low Frequency Vibration Isolator. Accepted for publication in *Defence Science Journal*, 2025.

[21] *ASTM D3580: A Standard for Vibration Test of Products* [online]. [viewed 2024-11-09]. Available from: https://1url.cz/8JMkV

[22] Rubber, Natural and Synthetic – General Test Methods; Carbon Black [online]. In: *Annual Book of ASTM Standards.* 2018, 09:01 [viewed 2024-11-20]. Available from: https://store.astm.org/astm-bos-09.01.html

[23] Rubber Products, Industrial – Specifications and Related Test Methods; Gaskets; Tires [online]. In: *Annual Book of ASTM Standards.* 2018, 09:02 [viewed 2024-11-20]. Available from: https://store.astm.org/astm-bos-09.02.html

[24] BROWN, R. *Physical Test Methods for Elastomers*. New York: Springer, 2018. ISBN 3-319-66726-2.

[25] TREVISO, A., B. VAN GENECHTEN, D. MUNDO and M. TOURNOUR. Damping in Composite Materials: Properties and Models. *Composites Part B: Engineering*. 2015, **78**(1), pp. 144-152. DOI 10.1016/j.compositesb.2015.03.081.

[26] GEETHAMMA, V.G., G. KALAPRASAD, G. GROENINCKX and T. SABU. Dynamic Mechanical Behaviour of Short Coir Fibre Reinforced Natural Rubber Composites. *Composites Part A: Applied Science and Manufacturing*, 2005, **36**(11), pp. 1499-1506. DOI 10.1016/j.compositesa.2005.03.004.

[27] TONG, X, Z. BAI and J. WU. Mechanical and Tribological Performance of Acrylonitrile-Butadiene Rubber/ Carbon Black/ Crypto Crystalline Graphite Composites. *Journal of Applied Polymer Science*, 2021, **138**(9), 49936. DOI 10.1002/app.49936.

[28] ZHAO, F. and R.J. FRANK. Thermal Loading of Short Fibre Composites and the Induction of Residual Shear Stresses. *Composites Part A: Applied Science and Manufacturing,* 2007, **38**(11), pp. 2374-2381. DOI 10.1016/ j.compositesa.2007.06.012.

[29] GLOWACKA, K., J. KLEMENC, M. NAGODE and T. LAGODA. Fatigue Lifetime of Rubber Composites–State-of-the-Art. *Polymer Testing,* 2025, **143**, 108713. DOI 10.1016/ j.polymertesting. 2025.108713.

[30] GOMEZ-JIMENEZ, S., T. SAUCEDO-ANAYA, C. GUERRERO-MENDEZ, A. ROBLES-GUERRERO, L. SILVA-ACOSTA, D. NAVARRO-SOLIS, D. LOPEZ-BETANCUR and A.R. CONTRERAS RODRÍGUEZ. Mooney-Rivlin Parameter Determination Model as a Function of Temperature in Vulcanized Rubber Based on Molecular Dynamics Simulations. *Materials*, 2024, **17**(13), 3252. DOI 10.3390/ma17133252.

[31] MARCHMANN, G. and E. VERON. Comparison of Hyperelastic Model for Rubber like Materials. *Rubber Chemistry and Technology*, 2006, **79**(5), pp. 835-858. DOI 10.5254/1.3547969.

[32] BHARAT. P.S., S.B. BARVE, S.G. THORAT and S.S. MAJUMDAR. Design and Analysis of Anti-Vibration Mount for G+3 Elevator. *International Journal of Current Engineering and Technology*, 2014, **3**, pp. 103-108. ISSN 2277-4106.

[33] ISO 10846-1. *Acoustics and Vibration – Laboratory Measurement of Vibro-Acoustic Transfer Properties of Resilient Elements – Part 1: Principles and Guidelines.*

[34] FODOR, B. and A. KOSSA. Stability Study of the Compressible Mooney-Rivlin Hyperelastic Model. *Journal of Strain Analysis for Engineering Design*, 2024, **59**(4), pp. 258-268. DOI 10.1177/03093247241233712.

[35] LI, K., G. CHEN, W. SUN, S. YAN, M. LI and B. LIU. Research on the Strength Calculation Method of Rubber Mount Housing for Heavy Truck Powertrain. *SAE Technical Paper Series,* 2024. DOI 10.4271/2024-01-5080.

[36] WANG W., C. SONG and X. LI. Finite Element Simulation Analysis of Static Stiffness of Bushing Rubber Mount. In: *Third International Conference on Advanced Manufacturing Technology and Manufacturing Systems*. Changsha: SPIE, 2024, pp. 978-982. DOI 10.1117/12.3038287.

[37] LI, Q., T. TANG, G. HE, M. YUAN and G. LI. Fatigue Life Prediction of a Rubber Mount Considering the Self-Heating by the Hysteresis Loss of the Rubber Material Subjected to Cyclic Loadings. *Journal of Macromolecular Science, Part B*, 2024, pp. 1-16. DOI 10.1080/00222348.2024.2393517.